

Directing the Self-Assembly of Conjugated Organic Ammonium Cations  
in Low-Dimensional Perovskites by Halide Substitution

Peer-reviewed author version

DENIS, Paul-Henry; Van Hecke, Kristof; VAN GOMPEL, Wouter; MERTENS, Martijn; RUTTENS, Bart; D'HAEN, Jan; LUTSEN, Laurence & VANDERZANDE, Dirk (2021) Directing the Self-Assembly of Conjugated Organic Ammonium Cations in Low-Dimensional Perovskites by Halide Substitution. In: Chemistry of materials, 33 (13) , p. 5177 -5188.

DOI: 10.1021/acs.chemmater.1c01221

Handle: <http://hdl.handle.net/1942/34672>

# Directing the self-assembly of conjugated organic ammonium cations in low-dimensional perovskites by halide substitution

Paul-Henry Denis,<sup>a†</sup> Martijn Mertens,<sup>a†</sup> Wouter T.M. Van Gompel,<sup>a</sup> Kristof Van Hecke,<sup>b</sup>

Bart Ruttens,<sup>c</sup> Jan D’Haen,<sup>c</sup> Laurence Lutsen,<sup>ac</sup> and Dirk Vanderzande<sup>\*ac</sup>

<sup>a</sup>Hybrid Materials Design (HyMaD), Institute for Materials Research (IMO-IMOMEC), Hasselt University, Martelarenlaan 42, B-3500 Hasselt, Belgium

<sup>b</sup>XStruct, Department of Chemistry, Ghent University, Krijgslaan 281-S3, B-9000 Ghent, Belgium

<sup>c</sup>Associated Laboratory IMOMEC, Imec, Wetenschapspark 1, B-3590 Diepenbeek, Belgium

**Corresponding author:** dirk.vanderzande@uhasselt.be

---

**ABSTRACT:** At present, two-dimensional (2D) hybrid organic-inorganic perovskites (HOIPs) are drawing significant interest due to their potential use in different optoelectronic applications, i.e., photovoltaics and photodetectors. Here, we report on a series of 2D layered HOIPs (Bit-C3)<sub>2</sub>PbX<sub>4</sub> (with X= Cl, Br, and I) containing a 2,2'-bithiophene chromophore functionalized with a propylammonium tethering chain as a model molecule. The optical properties, crystal structure, and phase behavior of the 2D layered HOIPs are studied in depth. The crystal structures with the chemical formula (Bit-C3)<sub>2</sub>PbX<sub>4</sub> (with X= Cl, and Br) were successfully obtained. Contrastingly, different crystal structures with an inorganic framework containing face- and corner-sharing octahedra were identified for the iodide-based HOIP. The phase diversity and thermal stability of the (Bit-C3)<sub>2</sub>PbX<sub>4</sub> (with X= Cl, Br and I) thin films were investigated *via in-situ* measurements. Here, the presence of lower-dimensional hybrids with reduced electronic dimensionality within the iodide-based thin film is demonstrated. Additionally, we show that the 2D hybrid thermal stability is dependent on the type of lead(II)halide framework employed. We suggest that *via* halide substitution from iodide to bromide and chloride, the molecular degrees of freedom of the Bit-C3 ammonium cations are reduced by spatial confinement of a smaller inorganic framework. Therefore, limiting the formation of lower-dimensional hybrids besides the targeted 2D layered HOIP. This study illustrates the importance of efficiently utilizing the space supplied by the inorganic framework in which the organic ammonium cations can reside within a 2D layered HOIP. This, in turn, dictates how the organic ammonium cations arrange themselves within the organic layer and influences the adopted crystal structure of the hybrid.

---

## INTRODUCTION

Two-dimensional (2D) layered hybrid organic-inorganic perovskites (HOIPs) continue to astonish the research community, owing to their practical use as active materials in various optoelectronic applications. They are composed of an alternation of organic layers and inorganic metal(II) halide corner-sharing octahedra sheets, generating a multiple quantum well structure by self-assembly. Notably, this layered architecture leads to a higher degree of compositional flexibility in the choice of the organic cations, which is not encountered in 3D HOIPs. Combined with the inherent environmental stability of 2D layered HOIPs, this enables the fabrication of a wide range of stable materials with attractive semiconducting properties.<sup>1-4</sup>

To date, 2D layered HOIPs are primarily based on large insulating aliphatic or aromatic ammonium cations (e.g., butyl or phenylethyl ammonium).<sup>3,5-7</sup> These simple organic cations possess a reasonably sizable gap between their frontier energy levels compared to the bandgap of the inorganic layer. As a consequence, the optical and electronic features of these materials

mainly arise from the metal(II) halide inorganic layers, which can be additionally tailored *via* halide substitution.<sup>8-16</sup>

When functional, semiconducting organic molecules are self-assembled within HOIPs, the hybrid material becomes entirely photoactive.<sup>8,17-24</sup> In this respect, oligothiophenes have been widely applied in organic electronics since their optoelectronic properties can be modified by functionalization or varying the conjugation length of the oligomer.<sup>25,26</sup> Likewise, oligothiophene derivatives have been explored within the field of 2D layered HOIPs as their energy levels closely match those of the metal(II) halide inorganic layers.<sup>10,16,27-31</sup> As a consequence, the structural and optoelectronic properties of 2D layered HOIPs can be tailored through compositional engineering.

2D layered HOIPs have been widely studied since the 1980's, and general principles for the synthesis and design are known for quite some time.<sup>32</sup> In this regard, prior work focused on the structure of the organic ammonium cation (i.e., alkyl chain length,<sup>33</sup> molecular bulkiness,<sup>34</sup> stacking behavior,<sup>35</sup> or presence of substituents<sup>28</sup>) and its impact on the self-assembly and

formation of 2D layered HOIPs. While halide substitution has been applied to tune the optoelectronic properties of HOIPs,<sup>10,11,16,27</sup> a comprehensive analysis of the influence of the lead(II) halide framework on the organic layer self-assembly has received less attention. Therefore, we studied the control of the inorganic framework's nature on the organic layer self-assembly and structure formation by halide substitution in detail. In this way, ascertaining the importance of the space supplied by the inorganic framework in which a particular organic ammonium cation can reside.

In this work, we report results on the synthesis and structural characterization of a series of 2D layered lead(II) halide HOIPs incorporating a 2,2'-bithiophene chromophore functionalized with a propylammonium (C3) tethering chain as a model molecule and vary the nature of the lead(II) halide inorganic framework *via* halide substitution (Fig. 1).

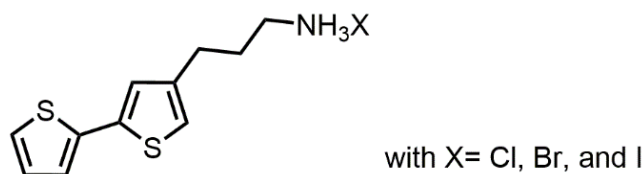


Figure 1. The structural formula of the 2,2'-bithiophene derivatives (Bit-C3)NH<sub>3</sub>X (with X= Cl, Br, and I).

The optical properties of (Bit-C3)<sub>2</sub>PbX<sub>4</sub> (with X= Cl, Br, and I) were investigated by absorption and photoluminescence emission spectroscopy. These results show an increase in inorganic excitonic band energy when substituting iodide with bromide and chloride. The 2D layered HOIP crystal structures of (Bit-C3)<sub>2</sub>PbBr<sub>4</sub> and (Bit-C3)<sub>2</sub>PbCl<sub>4</sub> were confirmed *via* single-crystal XRD. On the contrary, lower-dimensional crystal structures containing face- and corner-sharing octahedra were obtained for the iodide-based HOIP.

*In-situ* temperature-controlled absorption spectroscopy and X-ray diffraction (XRD) measurements were used to examine the phase behavior (i.e., formation/degradation) and diversity of the series of 2D layered HOIPs in thin films. It was confirmed that additional iodide-based hybrid phases with a reduced electronic dimensionality were present besides the targeted 2D layered HOIP. The number of adopted hybrid phases for a given lead(II) halide HOIP derivative decreases *via* halide substitution, from iodide to chloride. These findings suggest that spatial confinement of the Bit-C3 ammonium cations by a smaller lead(II) halide framework reduces the probability of obtaining additional lower-dimensional hybrids. To further assess the importance of the templating role and spatial confinement of the inorganic framework, different mixed halide (Bit-C3)<sub>2</sub>PbI<sub>4-4x</sub>Br<sub>4x</sub> HOIPs (with x= 0.025, 0.05, 0.25, 0.50, and 0.75) were prepared and analyzed. We demonstrate that when a 5 % bromide anion content is employed, the crystallization can be driven towards a 2D layered HOIP with optical properties closely related to those of the 2D hybrid (Bit-C3)<sub>2</sub>PbI<sub>4</sub>.

Our study demonstrates how the nature of the lead(II) halide framework can directly influence the self-assembly of the large organic ammonium cations and possibly steers the adopted crystal structure of the hybrid.

## RESULTS AND DISCUSSIONS

**Optical and structural properties.** The mono-functionalized organic ammonium cations (Bit-C3)NH<sub>3</sub>X (with X= Cl, Br, and I) were synthesized starting from a 2,2'-bithiophene

core (Supporting Fig. S1). The 2D layered HOIPs (Bit-C3)<sub>2</sub>PbX<sub>4</sub> (X=Cl, Br, and I) were prepared by mixing stoichiometric ratios of (Bit-C3)NH<sub>3</sub>X and PbX<sub>2</sub> in the suitable solvents. Afterward, the precursor solutions were spin-coated and annealed at 150 °C to obtain the desired crystalline thin films (Supporting Fig. S2). As the first indication of 2D layered HOIP formation, UV-Vis absorption spectra were measured. The 2D layered HOIPs (Bit-C3)<sub>2</sub>PbX<sub>4</sub> (X= Cl, Br, and I) are successfully synthesized based on the appearance of the excitonic absorption peaks originating from the inorganic layers consisting out of lead(II) halide corner-sharing octahedra (Fig. 2).

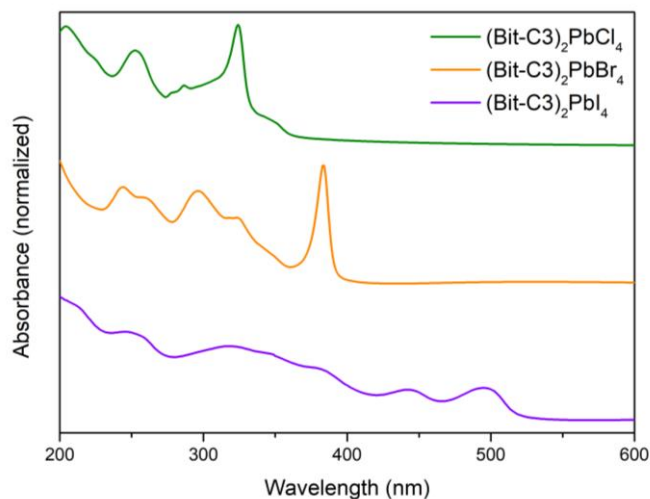


Figure 2. Absorption spectra of (Bit-C3)<sub>2</sub>PbX<sub>4</sub> (X= Cl, Br, and I) thin films annealed at 150°C for 15 min.

The regions in which the excitonic absorbance peaks appear for (Bit-C3)<sub>2</sub>PbCl<sub>4</sub> (324 nm), (Bit-C3)<sub>2</sub>PbBr<sub>4</sub> (383 nm), and (Bit-C3)<sub>2</sub>PbI<sub>4</sub> (500 nm) are characteristic for 2D layered lead(II) chloride, bromide, and iodide-based HOIPs respectively. The trend in excitonic band energy can be directly attributed to the change in nature of the employed halogen.<sup>12,16,20,27,36</sup> When comparing the series of 2D layered HOIPs, the excitonic absorption peak positions can be shifted from the near-UV towards the visible spectral region *via* halide substitution from chloride to iodide. Moreover, an additional excitonic absorption peak at 443 nm is present in the (Bit-C3)<sub>2</sub>PbI<sub>4</sub> film, corresponding to an undefined lower-dimensional phase (LD<sub>443</sub>).<sup>20</sup> The simultaneous presence of both hybrid phases with a broad excitonic absorption peak signal indicates that the crystallization towards one particular phase is inefficient.<sup>37,38</sup> The short-wavelength absorption features of the conjugated organic ammonium cations are also visible, which are in accordance with the ones obtained from the (Bit-C3)NH<sub>3</sub>X (X=Cl, Br, and I) salt thin films (Supporting Fig. S7).

The emission properties of the (Bit-C3)<sub>2</sub>PbX<sub>4</sub> (X=Cl, Br, and I) thin films were evaluated by photoluminescence (PL) emission spectroscopy (Supporting Fig S8). The emission spectra of the (Bit-C3)NH<sub>3</sub>X (X=Cl, Br, and I) thin films were added for comparison. For the emission spectra of (Bit-C3)<sub>2</sub>PbX<sub>4</sub> (with X= I and Br), the 2D hybrid excitonic emission peaks are visible at respectively 387 nm and 512 nm, in addition to the weak chromophore emission. As can be remarked, the excitonic emission peak intensity arising from the (Bit-C3)<sub>2</sub>PbI<sub>4</sub> thin film is low compared to (Bit-C3)<sub>2</sub>PbBr<sub>4</sub>. Note that the excitonic emission peak of LD<sub>443</sub> is absent, which may be attributed to energy funneling towards the 2D hybrid.<sup>39</sup>

For  $(\text{Bit-C3})_2\text{PbCl}_4$ , a strong chromophore emission centered at 395 nm is exclusively observed without the presence of an excitonic emission peak. This observation was also discerned for  $(\text{R-NH}_3)_2\text{PbCl}_4$  (R= phenylmethyl, 2-naphthylmethyl, and 2-anthrylmethyl)<sup>40</sup> or bis(aminoethyl)-quaterthiophene lead chloride (AEQT) $\text{PbCl}_4$ ,<sup>16</sup> showing energy transfer from the inorganic towards the organic component. As the singlet state ( $S_1$ ) of 2,2'-bithiophene (estimated at 3.83-3.88 eV)<sup>41</sup> lies energetically close to the inorganic excitonic band of  $(\text{Bit-C3})_2\text{PbCl}_4$  (3.83 eV), we propose that the intense chromophore emission could similarly be the result of energy transfer *via* exciton migration. Lastly, the intense chromophore emission of  $(\text{Bit-C3})_2\text{PbCl}_4$  is slightly blue-shifted compared to  $(\text{Bit-C3})_2\text{PbX}_4$  (with X= I and Br) and might be the result of a conformational change of the Bit-C3 ammonium cations within the different lead(II) halide inorganic frameworks.<sup>16</sup>

The XRD patterns of the spin-coated  $(\text{Bit-C3})_2\text{PbX}_4$  (X= Cl, Br, and I) thin films are shown in **Figure 3**. The diffraction patterns consist of a series of (0 0 l) reflections characteristic for a  $n = 1$  layered perovskite with a preferential growth along the [1 1 0] direction, parallel to the substrate surface.<sup>42</sup> These experimental patterns match with those of the simulated XRD patterns of the corresponding single-crystals (*vide infra*). The interplanar  $d_{001}$ -spacing values of the  $(\text{Bit-C3})_2\text{PbX}_4$  (X= Cl, Br, and I) thin films are represented in **Table 1**. The distance between subsequent inorganic lead(II) halide sheets increases by almost 5 Å, going from the 2D hybrid  $(\text{Bit-C3})_2\text{PbI}_4$  to  $(\text{Bit-C3})_2\text{PbCl}_4$ . For comparison, the length of a single Bit-C3 ammonium cation is ~ 13 Å (Chem3D, PerkinElmer Informatics). The calculated interplanar  $d$ -spacing values are based on spin-coated  $(\text{Bit-C3})_2\text{PbX}_4$  (X= Cl and Br) thin films annealed at 150 °C for 15 min. It has proven difficult to obtain the 2D hybrid phase separately without the presence of the LD<sub>443</sub> hybrid phase for a  $(\text{Bit-C3})_2\text{PbI}_4$  thin film annealed at 150°C. Therefore, an estimate of the interplanar  $d$ -spacing values for the two hybrid phases (2D, and LD<sub>443</sub>) was derived, based on the XRD patterns obtained from an *in-situ* temperature-controlled measurement on a  $(\text{Bit-C3})_2\text{PbI}_4$  thin film annealed at 30 °C for 5 min (see section 'phase formation/degradation behavior').

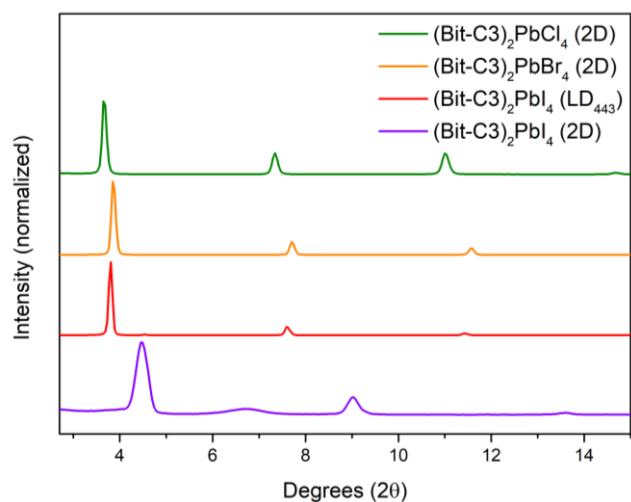


Figure 3 X-ray diffraction patterns of the spin-coated  $(\text{Bit-C3})_2\text{PbX}_4$  (X= Cl and Br) thin films annealed at 150 °C for 15 min and of a spin-coated  $(\text{Bit-C3})_2\text{PbI}_4$  thin film obtained from an *in-situ* temperature-controlled X-ray diffraction measurement (peak at ~ 6.6° 2θ is due to Kapton from the temperature chamber).

**Table 1. Interplanar  $d$ -spacing values of  $(\text{Bit-C3})_2\text{PbX}_4$  (X= Cl, Br, and I) thin films**

$(\text{Bit-C3})_2\text{PbX}_4$ (X= Cl, Br, and I)	Interplanar $d_{001}$ -spacing (Å)
$(\text{Bit-C3})_2\text{PbI}_4$ , 2D	19.9
$(\text{Bit-C3})_2\text{PbI}_4$ , LD <sub>443</sub>	23.4
$(\text{Bit-C3})_2\text{PbBr}_4$ , 2D	23.5
$(\text{Bit-C3})_2\text{PbCl}_4$ , 2D	24.7

The discerned trend in interplanar  $d$ -spacing can be further clarified by crystal structure determination of  $(\text{Bit-C3})_2\text{PbX}_4$  (with X= Cl, Br, and I) *via* single-crystal XRD. By utilizing an anti-solvent vapor diffusion crystallization approach,<sup>43</sup> we successfully obtained single-crystals with the chemical formula  $(\text{Bit-C3})_2\text{PbBr}_4$ , and  $(\text{Bit-C3})_2\text{PbCl}_4$  (**Fig. 4**). Unfortunately, we did not succeed in obtaining the 2D layered lead(II) iodide HOIP structure using this approach. Instead, a lower-dimensional hybrid was obtained, represented by a large unit cell (Supporting **Fig. S4**). In this crystal structure, the inorganic framework comprises corner- and face-sharing lead(II) iodide octahedra, forming a lower-dimensional hybrid instead of the targeted 2D layered crystal structure. The lower-dimensional hybrid crystallizes in the monoclinic crystal system with space group  $P2_1/c$ . The conjugated Bit-C3 ammonium cations adopt different conformations and interdigitate within the organic bilayer.

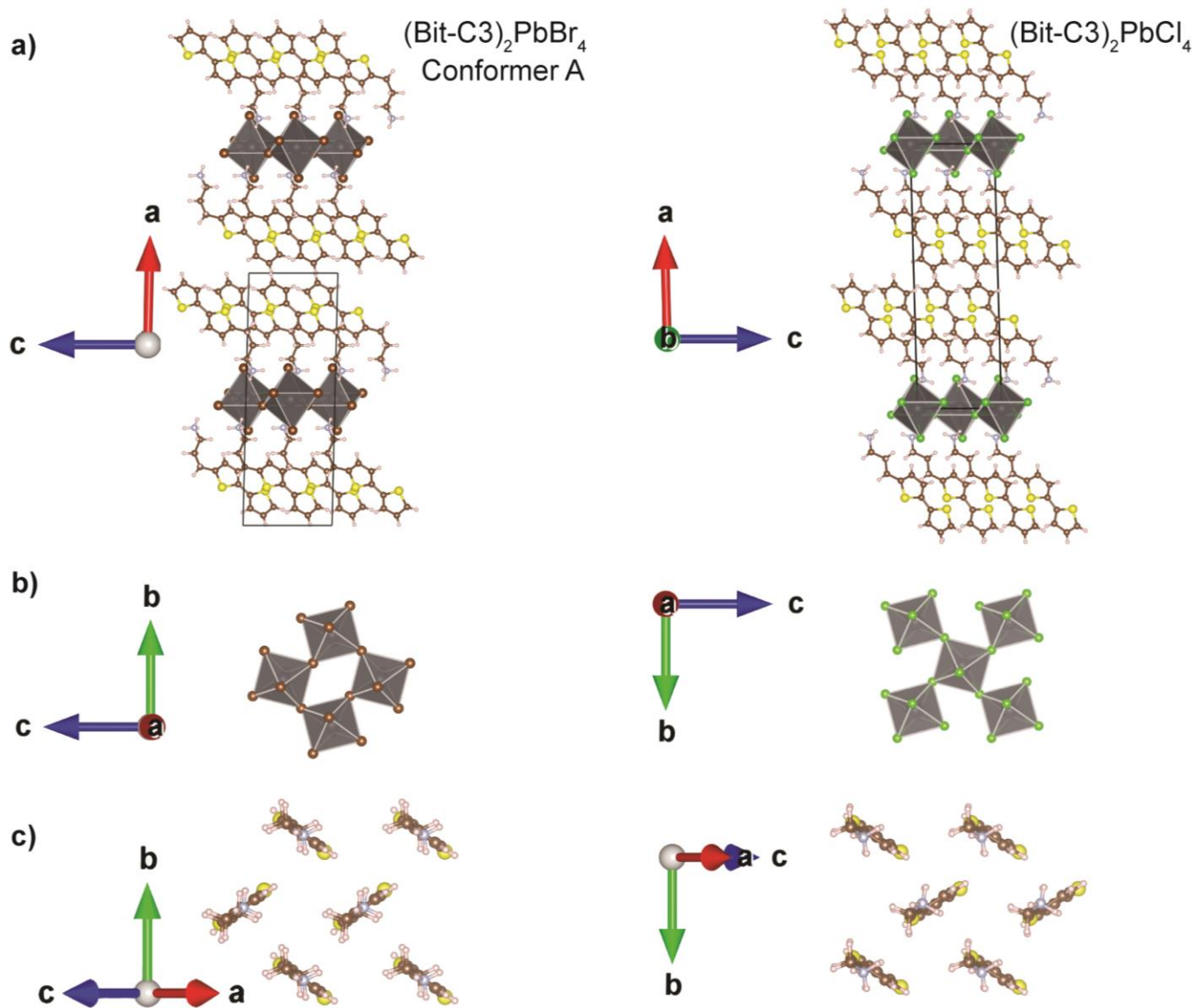


Figure 4. Illustration of the (a) side view, (b) interconnection of the octahedral sheets, and (c) perspective along the molecular axis of the Bit-C3 ammonium cations within the organic layer of  $(\text{Bit-C3})_2\text{PbBr}_4$ , and  $(\text{Bit-C3})_2\text{PbCl}_4$ . Only conformer A (bent) of the disordered Bit-C3 ammonium cations is shown in  $(\text{Bit-C3})_2\text{PbBr}_4$ . Conformer B (planar) can be found in supporting Fig. S3. The lead atoms are colored bright grey, the bromine atoms brown, the chlorine atoms light green, the nitrogen atoms light blue, the hydrogen atoms light pink, the carbon atoms dark orange, and the sulfur atoms yellow. This figure was made using VESTA.

Unfortunately, this crystal structure's simulated XRD pattern does not match the hybrid phases (2D, or LD<sub>443</sub>) encountered within a spin-coated (Bit-C3)<sub>2</sub>PbI<sub>4</sub> thin film annealed at 150°C. Importantly, this crystal structure contains significant voids, in which the cavity residing species could not be modeled. Remarkably, a 2D layered lead(II) iodide HOIP crystal structure containing a 2,2'-bithiophene mono-functionalized with ethyl instead of a propyl ammonium tethering chain was previously reported.<sup>28</sup> In contrast, a similar observation to ours was made when a 5-ammoniummethylsulfanyl-2,2'-bithiophene (AESBT) organic ammonium cation was employed, yielding a lower-dimensional crystal structure instead of the targeted 2D hybrid.<sup>31</sup> These experimental observations reflect on the importance of the alkyl chain length of the organic ammonium cation, influencing the formation of low-dimensional structures.<sup>33</sup> This seems to be less important for strongly stacking planar chromophores (e.g., pyrene-butylammonium<sup>19,20</sup>), and as we will demonstrate, for a more confined inorganic framework.

For the crystal structures of (Bit-C3)<sub>2</sub>PbX<sub>4</sub> (with X= Br, and Cl), the inorganic framework comprises exclusively corner-sharing lead(II) halide octahedra, forming the well-known '2D layered' crystal structure. Both HOIPs crystallize in the monoclinic crystal system with space group *P*2<sub>1</sub>/*c*. In these structures, the conjugated Bit-C3 ammonium cations do not interdigitate in the bilayer and adopt a herringbone arrangement. This arrangement is expected based on the quadrupole interactions of the 2,2'-bithiophene moieties inducing T-shape stacking. The simulated XRD patterns of these crystal structures are perfectly matching those of the spin-coated thin films. The cause of the increase in *d*-spacing, from (Bit-C3)<sub>2</sub>PbBr<sub>4</sub> to (Bit-C3)<sub>2</sub>PbCl<sub>4</sub>, becomes evident when comparing the conformational arrangement of the conjugated Bit-C3 ammonium cations in detail. For (Bit-C3)<sub>2</sub>PbBr<sub>4</sub>, the conjugated Bit-C3 ammonium cations are disordered over two conformations A and B with nearly the same probability of occurrence (Fig. 5; perovskite structures Supporting Fig. S3).

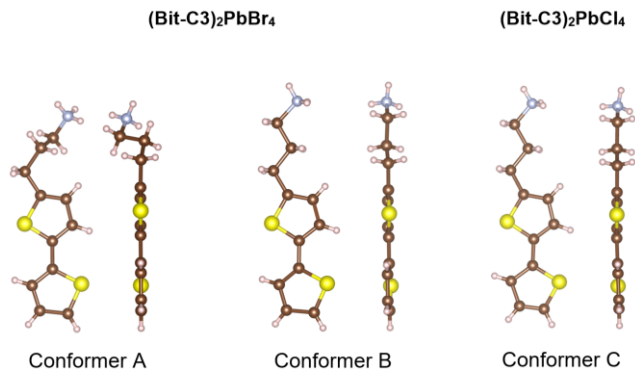


Figure 5. Different adopted conformations of the conjugated Bit-C3 ammonium cations inside the organic bilayer of (Bit-C3)<sub>2</sub>PbBr<sub>4</sub> (conformer A and B) and (Bit-C3)<sub>2</sub>PbCl<sub>4</sub> (conformer C). The nitrogen atoms are colored light blue, the hydrogen atoms light pink, the carbon atoms dark orange, and the sulfur atoms yellow. This figure was made using VESTA.

More precisely, the propyl ammonium chain of conformer A appears in a slightly bent conformation, leaving the carbon atom close to the ammonium group out of the 2,2'-bithiophene plane. In contrast, conformer B displays a planar conformation, in which the aliphatic carbon atoms are anti to each other and are in the plane of the 2,2'-bithiophene chromophore. In contrast, the conjugated Bit-C3 ammonium cations adopt one planar conformation in the crystal structure of (Bit-C3)<sub>2</sub>PbCl<sub>4</sub>, in which all

carbon atoms of the propyl ammonium chain are in the plane of the chromophore core (Conformer C, Fig. 5). Due to this planar conformation in (Bit-C3)<sub>2</sub>PbCl<sub>4</sub>, the *d*-spacing slightly increases from 23.5 to 24.7 Å compared to (Bit-C3)<sub>2</sub>PbBr<sub>4</sub>. The difference in the conformational arrangement can be related to the reduction in space available for an organic ammonium cation to be self-assembled within the inorganic framework. In this respect, the area defined by the terminal halides from four neighboring PbX<sub>6</sub><sup>4-</sup> octahedra diminishes when substituting bromide with chloride possessing a smaller ionic radius.<sup>44</sup> The area reduction becomes noticeable when comparing the unit cell constants *a*, *b*, and *c* of the crystal structures (Table 2). Additionally, the lattice parameters reported by Gao *et al.*<sup>28</sup> of a 2D layered lead(II) iodide HOIP crystal structure containing 2,2'-bithiophene mono-functionalized with ethyl (Bit-C2) instead of propyl were added to complete the series of results. We will apply this 2D hybrid structure of (Bit-C2)<sub>2</sub>PbI<sub>4</sub> to approximate the one of (Bit-C3)<sub>2</sub>PbI<sub>4</sub>, which could not be obtained.

Table 2. Crystallographic data of (Bit-C2)<sub>2</sub>PbI<sub>4</sub><sup>28</sup> and (Bit-C3)<sub>2</sub>PbX<sub>4</sub> (with X= Br and Cl)

Unit cell parameters	(Bit-C2) <sub>2</sub> PbI <sub>4</sub>	(Bit-C3) <sub>2</sub> PbBr <sub>4</sub>	(Bit-C3) <sub>2</sub> PbCl <sub>4</sub>
<i>a</i> (Å)	12.0865(13)	23.5063(5)*	24.7740(5)*
<i>b</i> (Å)	12.2697(12)	7.7046(2)	7.35765(14)
<i>c</i> (Å)	20.808(2)*	8.2879(2)	7.86657(15)
<i>V</i> (Å <sup>3</sup> )	3016.1(5)	1500.59(6)	1433.37(5)

\* The layer growth of (Bit-C2)<sub>2</sub>PbI<sub>4</sub> occurs along the [001] direction (*c*-axis), whereas in (Bit-C3)<sub>2</sub>PbX<sub>4</sub> (with X=Br and Cl) along the [100] direction (*a*-axis).

By substituting bromide into chloride in (Bit-C3)<sub>2</sub>PbX<sub>4</sub>, the unit cell constants *b* and *c* are reduced in the layer growth (100) plane, whereas *a* increases along the layer growth [100] direction. Particularly inducing a reduction in unit cell volume, from ~ 1500 to 1433 Å<sup>3</sup>. Extrapolating these findings towards the 2D hybrid of (Bit-C3)<sub>2</sub>PbI<sub>4</sub> with a likely reduced *d*-spacing of 19.9 Å (from thin film XRD) would imply that the unit cell constants *b* and *c* increase even further with respect to (Bit-C3)<sub>2</sub>PbBr<sub>4</sub>, due to the larger iodide anion radius. For the literature crystal structure of (Bit-C2)<sub>2</sub>PbI<sub>4</sub>, the unit cell volume increases dramatically due to the increased unit cell constants *a* and *b* in the layer growth (001) plane, even if the lattice constant *c* reduces along the layer growth [001] direction. Going from Bit-C2 towards Bit-C3, assuming a planar conformation, would increase the unit cell constants along the layer growth direction with approximately 2.2 Å to yield a *d*-spacing of 23 Å (obtained from the addition of a CH<sub>2</sub>-group to the alkyl tethering chain in the organic bilayer: 2 x 1.1 Å). This calculation is in line with the series of (Bit-C3)<sub>2</sub>PbX<sub>4</sub> (X=Br and Cl). The *d*-spacing of the 2D (Bit-C3)<sub>2</sub>PbI<sub>4</sub> (19.9 Å) obtained in thin film, points to a quite different packing of the Bit-C3 ammonium cations in the organic layer compared to (Bit-C3)<sub>2</sub>PbX<sub>4</sub> (X= Br and Cl). The increased (Bit-C2)<sub>2</sub>PbI<sub>4</sub> unit cell volume may explain such different packing, as it leaves the organic ammonium cations with more molecular degrees of freedom within the area defined by the terminal iodides from four neighboring lead(II) iodide octahedra (Fig. 6).

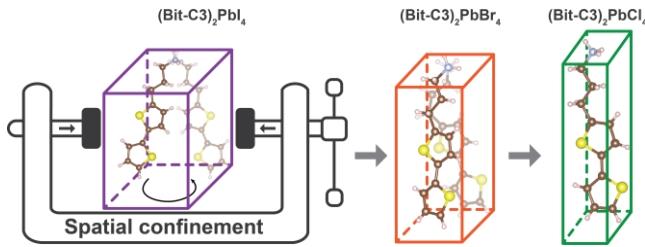


Figure 6. Spatial confinement of the inorganic framework. The adopted Bit-C3 ammonium cation conformations are represented in each unit cell of the series of  $(\text{Bit-C3})_2\text{PbX}_4$  ( $X = \text{I}, \text{Br}, \text{and Cl}$ ). Note that in the schematic, the actual molecular size of the Bit-C3 ammonium cations is exaggerated within each unit cell, and the unit cell dimensions are not drawn to scale.

Based on the obtained crystal structures of the iodide-based HOIP, reorganization of the corner-sharing lead(II) iodide octahedra can occur as well, involving the formation of additional edge- or face-sharing octahedral networks. As a result, the increasing trend in  $d$ -spacing of the 2D hybrids  $(\text{Bit-C3})_2\text{PbX}_4$  (with  $X = \text{Cl}, \text{Br}, \text{and I}$ ) within spin-coated thin films, in the order of  $\text{I}$  ( $19.9 \text{ \AA}$ ) <  $\text{Br}$  ( $23.5 \text{ \AA}$ ) <  $\text{Cl}$  ( $24.7 \text{ \AA}$ ), can be supported by the reduced molecular degrees of freedom of the Bit-C3 ammonium cations due to spatial confinement of the inorganic framework along the layer (100) plane. This reflects the importance of the inorganic framework's templating effect, which is additionally guided by hydrogen bonding between the halides of the perovskite framework and the terminal ammonium groups of the Bit-C3 molecules.<sup>8,45</sup> We, therefore, propose that the reduced molecular degrees of freedom of the Bit-C3 ammonium cations minimizes the chance of obtaining lower-dimensional hybrids. Likewise, by going from a propyl to an ethyl ammonium tethering chain, the molecular degrees of freedom of the organic ammonium cations are reduced, steering the crystallization towards the 2D hybrid  $(\text{Bit-C2})_2\text{PbI}_4$ . The detailed crystallographic information of the crystal structures can be found in the supporting information.

**Phase formation/degradation behavior** As previously depicted, the  $\text{LD}_{443}$  hybrid phase is present besides the targeted 2D hybrid phase within a spin-coated  $(\text{Bit-C3})_2\text{PbI}_4$  thin film annealed at  $150 \text{ }^\circ\text{C}$ . We hypothesize that increasing the dimensions of the unit cell, relaxes the restrictions on the conformation a Bit-C3 ammonium cation can adopt within the inorganic framework, hence, increasing the phase diversity (i.e. promoting the formation of other lower-dimensional hybrids). To confirm this hypothesis, *in-situ* temperature-controlled UV-Vis absorption, and XRD measurements were carried out, starting from a spin-coated film of  $(\text{Bit-C3})_2\text{PbX}_4$  (with  $X = \text{Cl}, \text{Br}, \text{and I}$ ) dried at  $30 \text{ }^\circ\text{C}$  for 5 min. In this way, a whole temperature range is examined to observe the possible presence of additional lower-dimensional hybrid phases, which are difficult to obtain in thin films annealed at one particular temperature. Likewise, the degradation behavior of the series of  $(\text{Bit-C3})_2\text{PbX}_4$  (with  $X = \text{Cl}, \text{Br}, \text{and I}$ ) thin films is studied. In this way, we can examine the influence of the lead(II)halide inorganic framework on the thermal stability of the respective 2D layered HOIPs. For the *in-situ* temperature-controlled UV-Vis absorption measurements, the samples were heated with incremental steps of  $1 \text{ }^\circ\text{C}$  per min until  $210 \text{ }^\circ\text{C}$ . In contrast, the XRD patterns were acquired during an isothermal period of 30 min every  $10 \text{ }^\circ\text{C}$ . A plot of the absorbance at the wavelengths of the excitonic absorption peaks as a function of temperature was made to clarify some observed trends.

Based on the *in-situ* measurements of a  $(\text{Bit-C3})_2\text{PbI}_4$  thin film (Fig. 7-8), the weakly crystalline 2D hybrid phase (500 nm, 7a) with a  $d$ -spacing of  $19.9 \text{ \AA}$  forms at relatively low temperatures and becomes predominant at  $110 \text{ }^\circ\text{C}$ .

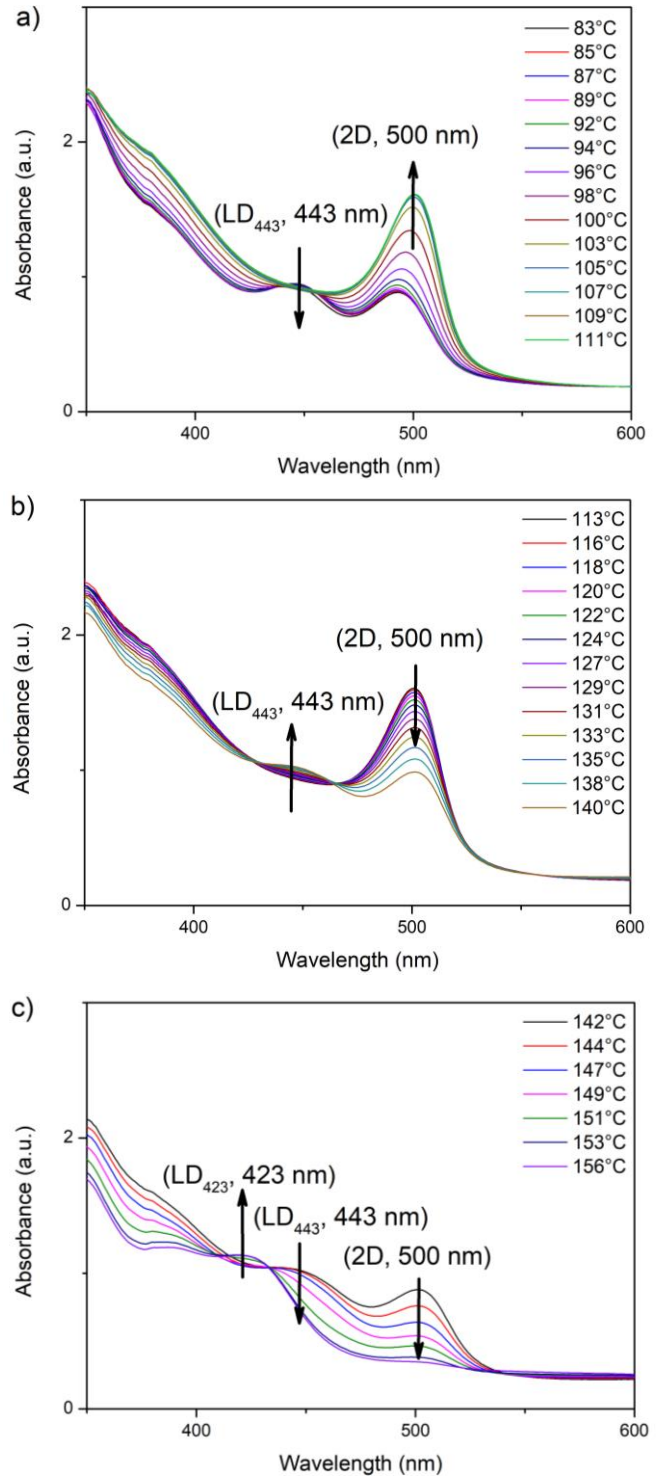


Figure 7. Absorption spectra as a function of temperature starting from a spin-coated film of  $(\text{Bit-C3})_2\text{PbI}_4$  dried at  $30 \text{ }^\circ\text{C}$  for 5 min before the *in-situ* experiment: (a) between  $83 \text{ }^\circ\text{C}$  and  $111 \text{ }^\circ\text{C}$ , (b) between  $113 \text{ }^\circ\text{C}$  and  $140 \text{ }^\circ\text{C}$ , and (c) between  $142 \text{ }^\circ\text{C}$  and  $156 \text{ }^\circ\text{C}$ . The arrows indicate whether the excitonic absorption peak increases or decreases over a specific temperature range. The peak wavelength is shown between brackets.

From thereon, the 2D hybrid phase slowly converts to a more crystalline LD<sub>443</sub> hybrid phase (443 nm, **7b**) with a larger *d*-spacing of 23.4 Å until 140 °C. The simultaneous presence of both hybrid phases indicates that the crystallization towards one particular hybrid is inefficient. After that, the LD<sub>443</sub> hybrid phase degrades between 140 and 160 °C into another lower-dimensional hybrid (LD<sub>423</sub>, 423 nm, **7c**) with a *d*-spacing of 20.1 Å. The thin film undergoes complete degradation into lead iodide (baseline increase in the absorption spectrum in the region of 520 nm, Supporting Fig. S10; diffractogram: main reflection at ~ 12,6° 2θ, Supporting Fig. S13).<sup>46</sup>

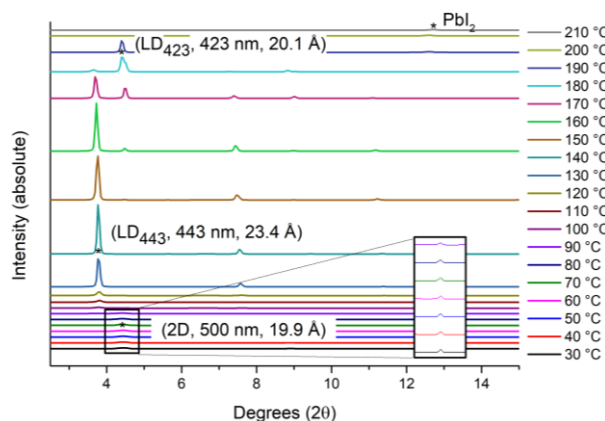


Figure 8. X-ray diffraction patterns (absolute) as a function of temperature starting from a spin-coated thin film of (Bit-C3)<sub>2</sub>PbI<sub>4</sub> dried at 30 °C for 5 min before the *in-situ* experiment. The weak reflections of the 2D hybrid phase are magnified in the temperature range between 30 and 90 °C.

The exact temperature at which a phase transition occurs differs between the two *in-situ* techniques, which can be explained by the difference in how temperature is measured. In the *in-situ* absorption spectroscopy setup, a thermocouple touches the film, while in the *in-situ* XRD setup, the temperature of the heating chamber is measured. By utilizing a layered solution crystal growth method,<sup>47</sup> a crystal structure was synthesized with the chemical formula (Bit-C3)<sub>3</sub>Pb<sub>2</sub>I<sub>7</sub>·H<sub>2</sub>O. Based on the comparison between the simulated XRD pattern of these crystals and the *in-situ* XRD pattern of the LD<sub>423</sub> hybrid phase (Supporting Fig. S5), the LD phase potentially resembles this crystal structure. The crystal structure possesses a 'lower-dimensional' inorganic framework containing corner- and face-sharing octahedra. However, these crystals also include one water molecule per unit cell, which will probably not be present in the LD hybrid phase of a spin-coated thin film annealed at 160 °C.

For the (Bit-C3)<sub>2</sub>PbBr<sub>4</sub> thin film, a reduction in phase diversity is noticeable compared to (Bit-C3)<sub>2</sub>PbI<sub>4</sub> (Fig. 9). Two hybrid phases are present with corresponding excitonic absorption peak positions of 382 and 393 nm and *d*-spacing values of 24 Å and 20.6 Å (Fig. 10). The 2D hybrid phase with an excitonic absorption peak at 382 nm undergoes a phase transition to another (likely very closely related) 2D hybrid phase with an excitonic absorption peak at 393 nm. However, this newly formed 2D hybrid phase shows relatively weak reflections compared to the initial one, indicating that it is relatively less crystalline or less strongly oriented.

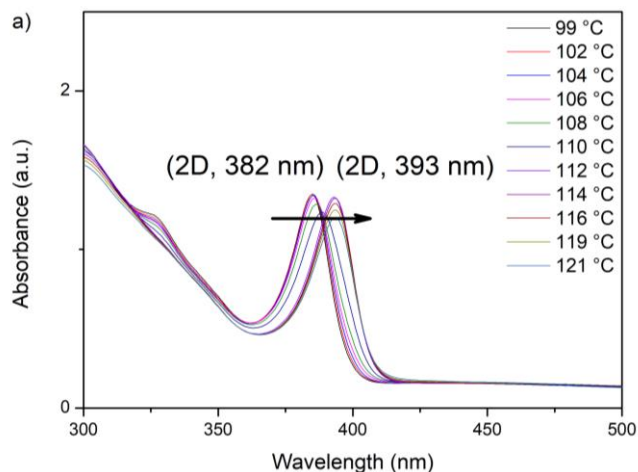


Figure 9. Absorption spectra as a function of temperature, between 99 °C and 121 °C, starting from a spin-coated film of (Bit-C3)<sub>2</sub>PbBr<sub>4</sub> dried at 30 °C for 5 min before the *in-situ* experiment. The peak wavelength is shown between brackets.

The small excitonic peak shift implies retention of the 2D structural dimensionality and a change in the distortion of the interconnected lead(II) bromide octahedra, possibly due to a small conformational change of the Bit-C3 ammonium cations.<sup>8,48</sup> Notice the slightly larger *d*-spacing corresponding to the 2D hybrid phase (382 nm) in the *in-situ* measurement compared to the *d*-spacing of a spin-coated thin film measured at room temperature. This increase in *d*-spacing is likely due to the thermal lattice expansion of the hybrid perovskite at high temperatures. These *in-situ* measurements demonstrate that the 2D hybrid phase directly degrades into an amorphous phase without the presence of intermediary steps *via* the formation of lower-dimensional hybrids as is the case for the iodide-based HOIP.

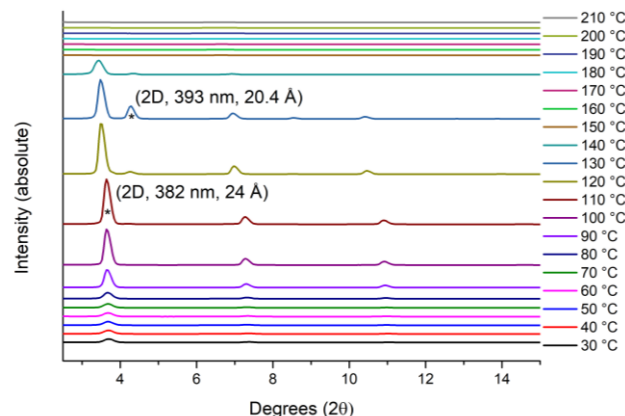


Figure 10. X-ray diffraction patterns (absolute) as a function of temperature starting from a spin-coated thin film of (Bit-C3)<sub>2</sub>PbBr<sub>4</sub> dried at 30 °C for 5 min before the *in-situ* experiment.

Finally, a single 2D hybrid phase of (Bit-C3)<sub>2</sub>PbCl<sub>4</sub> with a *d*-spacing of 25 Å is apparent from the *in-situ* temperature-controlled UV-Vis (Fig. 11a-b) and XRD measurements (Fig. 12). This phase forms at low temperatures but gradually degrades into an amorphous phase when the temperature is ramping up. Both *in-situ* measurements demonstrate the relatively low intrinsic thermal stability of (Bit-C3)<sub>2</sub>PbCl<sub>4</sub> compared to (Bit-C3)<sub>2</sub>PbX<sub>4</sub> (with X= I and Br). We suggest that this could be related to the relatively narrow space supplied by the lead(II) chloride inorganic framework, in which the conformational degrees of freedom of the Bit-C3 ammonium cations are lowered.

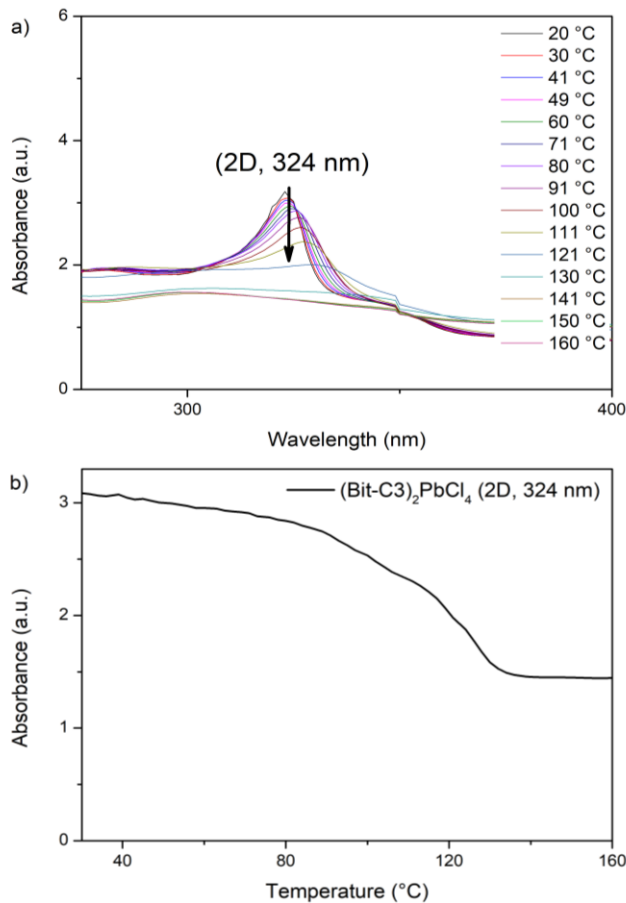


Figure 11. (a) Absorption spectra as a function of temperature, between 20 °C and 160 °C, starting from a spin-coated film of  $(\text{Bit-C3})_2\text{PbCl}_4$  dried at 30 °C for 5 min before the *in-situ* experiment. The black arrow indicates that the excitonic absorption peak at 324 nm decreases with temperature in this range due to thermal degradation. (b) Absorbance at 324 nm as a function of temperature, extracted from the absorption spectra at different temperatures.

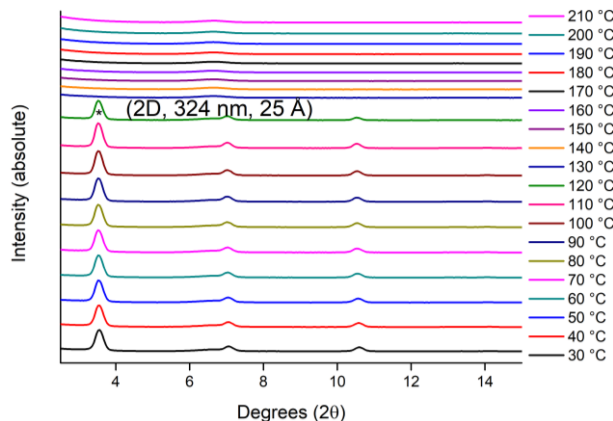


Figure 12. X-ray diffraction patterns (absolute) as a function of temperature starting from a spin-coated thin film of  $(\text{Bit-C3})_2\text{PbCl}_4$  that was dried at 30 °C for 5 min before the *in-situ* experiment.

Overall, a clear decrease in phase diversity of the 2D layered HOIPs is noticeable when the halide is substituted from iodide into bromide and chloride indicating the templating role of the inorganic framework in controlling the formation of additional lower-dimensional hybrid phases. The absence of any lower-dimensional hybrid phase for the bromide or chloride-based HOIPs implies that there could be increased 'strain' in the

inorganic framework of the 2D hybrid, which leads directly to thermal degradation into an amorphous phase without any intermediate phase formation. The remaining *in-situ* temperature-controlled UV-Vis spectra (Supporting Fig. S9-12) and *in-situ* XRD patterns with normalized intensities (Supporting Fig. S13-15) of the different thin film samples are shown in the ESI for completeness and clarity.

**Mixed halide lead(II) - based 2D layered HOIPs.** We showed that the phase diversity of  $(\text{Bit-C3})_2\text{PbX}_4$  (with  $\text{X}=\text{Cl}$ ,  $\text{Br}$ , and  $\text{I}$ ) could be diminished *via* halide substitution from iodide to bromide and chloride. To study the phase behavior of 2D layered HOIPs more in-depth and demonstrate the importance of the inorganic framework's templating effect, a series of mixed halide 2D layered HOIPs  $(\text{Bit-C3})_2\text{PbI}_{4-4x}\text{Br}_{4x}$  (with  $x=0.025, 0.05, 0.25, 0.50$ , and  $0.75$ ) was synthesized. The precursor solutions of  $(\text{Bit-C3})_2\text{PbI}_{4-4x}\text{Br}_{4x}$  were prepared by mixing stoichiometric ratios of the lead salts  $\text{PbX}_2$  and Bit-C3 ammonium salts  $(\text{Bit-C3})\text{NH}_3\text{X}$  (with  $\text{X}=\text{I}$  and  $\text{Br}$ ) in dry DMF and were spin-coated afterward. The thin films were annealed at 150 °C to obtain the desired crystalline materials. The UV-Vis absorption spectra of the different mixed halide HOIPs are shown in Figure 13.

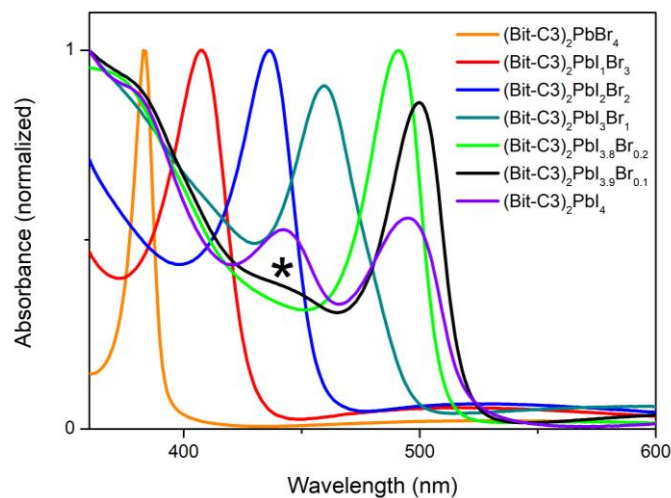


Figure 13. Absorption spectra of  $(\text{Bit-C3})_2\text{PbI}_{4-4x}\text{Br}_{4x}$  thin films (with  $x=0, 0.025, 0.05, 0.25, 0.5, 0.75$ , and  $1$ ) annealed at 150 °C for 15 min. The LD<sub>443</sub> phase of the iodide-based HOIP is highlighted with an asterisk. Note that the spectra of  $(\text{Bit-C3})_2\text{PbI}_4$  and  $(\text{Bit-C3})_2\text{PbBr}_4$  were added to complete the sequence in halide compositions.

As is apparent, the excitonic absorption peak gradually shifts from 500 to 382 nm by increasing the bromide anion content within the mixed halide 2D layered HOIP. More importantly, the additional excitonic absorption peak of the LD<sub>443</sub> phase of  $(\text{Bit-C3})_2\text{PbI}_4$  already disappears when a 5 % bromide anion content is employed. When the bromide anion content is reduced to 2.5 %, the excitonic peak of the LD<sub>443</sub> phase is still slightly present (Fig. 13, asterisk). Compared to the single halide 2D layered HOIP  $(\text{Bit-C3})_2\text{PbI}_4$ , the excitonic absorption peak of  $(\text{Bit-C3})_2\text{PbI}_{3.8}\text{Br}_{0.2}$  slightly shifts towards a lower wavelength (from 500 to 491 nm). When plotting the wavelengths at which the excitonic absorption peaks appear in function of iodide anion content, an almost linear trend is achieved (Fig. 14). The linearity confirms that the series of HOIPs possess a similar 2D structural dimensionality over the entire halide composition range.

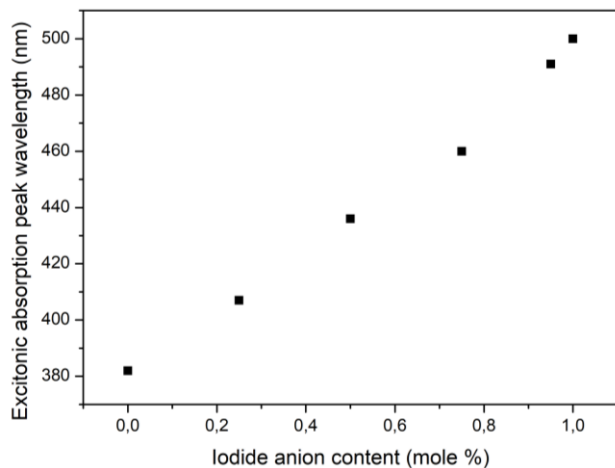


Figure 14. Excitonic absorption peak wavelength as a function of iodide anion content, extracted from the absorption spectra of a spin-coated  $(\text{Bit-C3})_2\text{PbI}_{4-4x}\text{Br}_{4x}$  thin film (with  $x = 0, 0.05, 0.25, 0.5, 0.75, 1$ ) annealed at  $150^\circ\text{C}$  for 15 min. Linear fitting with adjusted R-squared of 0.99.

If lower-dimensional phases had been formed instead upon halide substitution, an additional shift in excitonic absorption peak (towards a lower wavelength) would be present.<sup>20,49</sup>

The XRD patterns of the  $(\text{Bit-C3})_2\text{PbI}_{4-4x}\text{Br}_{4x}$  thin films (with  $x = 0, 0.025$  and  $0.05$ ) are compared (Fig. 15). Besides the predominant  $\text{LD}_{443}$  phase ( $23.4 \text{ \AA}$ ) present in a  $(\text{Bit-C3})_2\text{PbI}_4$  thin film, some weak reflections of the 2D ( $19.9 \text{ \AA}$ ) and  $\text{LD}_{423}$  hybrid ( $20.1 \text{ \AA}$ ) are noticeable. For the  $(\text{Bit-C3})_2\text{PbI}_{3.8}\text{Br}_{0.2}$  thin film, the XRD pattern reveals a single 2D hybrid phase.

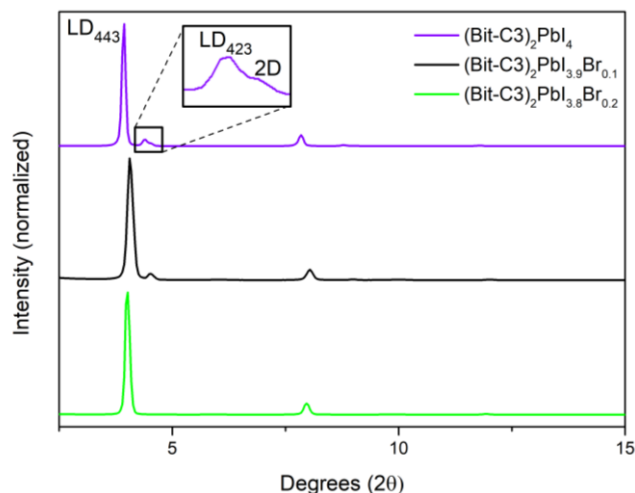


Figure 15. X-ray diffraction patterns of the spin-coated  $(\text{Bit-C3})_2\text{PbI}_{4-4x}\text{Br}_{4x}$  thin films (with  $x = 0, 0.025, \text{ and } 0.05$ ), annealed at  $150^\circ\text{C}$  for 15 min.

The  $d$ -spacing ( $22 \text{ \AA}$ ) of the 2D hybrid containing 5% bromide is increased compared to that of the 2D hybrid of  $(\text{Bit-C3})_2\text{PbI}_4$  ( $19.9 \text{ \AA}$ ) in thin film. Here, the suppression of the  $\text{LD}_{443}$  and  $\text{LD}_{423}$  hybrid phase within a  $(\text{Bit-C3})_2\text{PbI}_4$  thin film can be accomplished using a minimal bromide anion content of 5% for the mixed iodide-bromide perovskite system. This yields exclusively a 2D hybrid, which approximates the exciton absorption peak of the 2D layered  $(\text{Bit-C3})_2\text{PbI}_4$  HOIP. Peculiarly, the  $d$ -spacing of  $22 \text{ \AA}$  closely matches with the calculated value of  $23 \text{ \AA}$ , obtained from the addition of a  $\text{CH}_2$ -group to the

alkyl tethering chain in the organic bilayer ( $2 \times 1.1 \text{ \AA}$ ) of  $(\text{Bit-C2})_2\text{PbI}_4$  (*vide supra*).

We attempted to synthesize single-crystals out of a  $(\text{Bit-C3})_2\text{PbI}_{3.8}\text{Br}_{0.2}$  precursor solution utilizing the anti-solvent vapor diffusion crystallization approach. Unfortunately, a lower-dimensional hybrid with chemical formula  $(\text{Bit-C3})_4\text{Pb}_3\text{I}_{10}$  was obtained instead of the targeted 2D hybrid (Supporting Fig. S6). Peculiarly, no bromide anions are incorporated in this crystal structure's inorganic framework (consisting of corner and face-sharing octahedra), contrary to the  $(\text{Bit-C3})_2\text{PbI}_{3.8}\text{Br}_{0.2}$  thin film, where it contributes to a shift in excitonic peak position. Consequently, the crystallization behavior from solution to yield single-crystals differs considerably from the one observed from spin-coating into thin films.

## CONCLUSIONS

We have reported the synthesis, optical properties, crystal structure, and phase behavior of a series of 2D layered lead(II) halide HOIPs  $(\text{Bit-C3})_2\text{PbX}_4$  (with  $X = \text{Cl, Br, and I}$ ). The shift in excitonic band energy from the near UV to the visible spectral region is attributed to the change in halide anion. The crystal structures with the chemical formula  $(\text{Bit-C3})_2\text{PbX}_4$  (with  $X = \text{Cl, and Br}$ ) were successfully obtained. However, a variety of crystal structures was found for the iodide-based hybrid with an inorganic framework containing both face- and corner-sharing octahedra. We have demonstrated how the nature of the lead(II) halide framework can directly influence the self-assembly of large organic ammonium cations. The inorganic framework allows for a modulation of the molecular degrees of freedom of the organic ammonium cations. In this way, the possible conformations an organic ammonium cation can adopt, are determined by the inorganic framework. This modulation leads to a decrease in phase diversity in the crystal structure as one moves from iodide to bromide and chloride. Furthermore, it was demonstrated that the substitution of a small amount of iodide into bromide anion content can induce a substantial reduction of lower-dimensional hybrids next to the desired iodide-based 2D layered HOIP in thin film. To conclude, we have provided a detailed analysis of the impact that halide substitution has on the formation of 2D layered HOIPs. Here, the inorganic framework's nature steers the organic layer self-assembly due to spatial restrictions.

## EXPERIMENTAL SECTION

**Chemicals and reagents.** Lead iodide ( $\text{PbI}_2$ , 99.999%) and lead chloride ( $\text{PbCl}_2$ , 99.999%) were either obtained from Lumtec or TCI (99.99%). Lead bromide ( $\text{PbBr}_2$ , 99.999%) was obtained from Aldrich. The lead halides were used without further purification. 1,3-Dibromopropane (98%) and gamma-butyrolactone (GBL, >99%) were obtained from TCI. Hydroiodic acid (HI, 57% w/w aq., distilled, unstabilized), tributylphosphate (TBP, 99%), phenethylamine (PEA, 99%), *n*-butyllithium (1.6 M solution in hexanes), dimethylformamide (DMF), methyl sulfoxide (DMSO, 99.7+%, Extra Dry) and methanol (99.9%, Extra dry) were purchased from Acros Organics. Hydrazine monohydrate (65%), hydrobromic acid (HBr, 48% w/w aq.), and all solvents used for synthesis (reagent grade) were purchased from Fisher Scientific. Potassium phthalimide salt (95%) and 2,2'-bithiophene (98%) were purchased from Fluorochem. Hydrochloric acid (HCl, 37% w/w, aq.) was purchased from VWR. All solvents and reagents were used as received. The dry DMF that was used to make the

precursor solutions, dichloromethane (DCM), and diethyl ether (Et<sub>2</sub>O) were obtained from a solvent purification system (MBRAUN SPS-800).

**Synthesis of (Bit-C3)NH<sub>3</sub>X salts (with X= Cl, Br, and I).** Detailed in the supporting information.

**Single-crystal growth.** For the growth of the single-crystals with an empirical formula of (Bit-C3)<sub>12</sub>Pb<sub>9</sub>I<sub>30</sub> using the anti-solvent vapor crystallization approach,<sup>43</sup> stoichiometric amounts [targeted (Bit-C3)<sub>2</sub>PbI<sub>4</sub> structure] of (Bit-C3)NH<sub>3</sub>I (0,0501 mmol) and PbI<sub>2</sub> (0.02505 mmol) were dissolved in dry GBL (0.5 mL) under continuous stirring at 40 °C for 30 min. The precursor solution was filtered through a syringe filter (0.2 μm mash) and transferred to a small glass vial (20 mL volume). The small vial was put in a larger brown glass vial (100 mL volume). Dichloromethane (10 mL) was injected in the gap between the two vials and the larger vial was capped off with a plastic cap and parafilm. The vials were left undisturbed in an incubator at 20 °C. After 5 days, the crystals were harvested for single-crystal X-ray diffraction analysis. These crystals were washed three times with dry diethyl ether and were dried under reduced pressure at RT.

For the growth of the single-crystals with an empirical formula of (Bit-C3)<sub>3</sub>Pb<sub>2</sub>I<sub>7</sub>·(H<sub>2</sub>O), a layered solution crystal growth technique was employed.<sup>47</sup> PbI<sub>2</sub> (0.5 mmol) was dissolved in 5 mL HI (57% w/w aq.)\* in a glass test tube. A solution of (Bit-C3)NH<sub>2</sub> (1 mmol) in 10 mL dry methanol was placed on top of the acidic solution. The glass test tube was left undisturbed in an incubator at 20 °C. After one day of crystal growth, the grown needle-like crystals on the layered interface were removed, washed with dry diethyl ether, and dried overnight under reduced pressure at RT.

\* HI was purified by extraction (3 x chloroform/TBP 10/1).<sup>29</sup>

For the growth of the single-crystals with an empirical formula of (Bit-C3)<sub>2</sub>PbBr<sub>4</sub>, using the anti-solvent vapor crystallization approach,<sup>43</sup> stoichiometric amounts of (Bit-C3)NH<sub>3</sub>Br (0.0572 mmol) and PbBr<sub>2</sub> (0.0286 mmol) were dissolved in dry DMF (1 mL) under continuous stirring at 40 °C for 30 min. The precursor solution was filtered through a syringe filter (0.2 μm mash) and transferred to a small glass vial (20 mL volume). The small vial was put in a larger brown glass vial (100 mL volume). Dichloromethane (10 mL) was injected in the gap between the two vials and the larger vial was capped off with a plastic cap and parafilm. The vials were left undisturbed in an incubator at 20 °C. After 6 days, the crystals were harvested for single-crystal X-ray diffraction analysis. These crystals were washed three times with dry diethyl ether and were dried under reduced pressure at RT.

For the growth of the single-crystals with an empirical formula of (Bit-C3)<sub>2</sub>PbCl<sub>4</sub>, using the anti-solvent vapor crystallization approach,<sup>43</sup> stoichiometric amounts of (Bit-C3)NH<sub>3</sub>Cl (0.0504 mmol) and PbCl<sub>2</sub> (0.0252 mmol) were dissolved in dry DMF (0.8 mL) under continuous stirring at 40 °C for 30 min. The precursor solution was filtered through a syringe filter (0.2 μm mash) and transferred to a small glass vial (20 mL volume). The small vial was put in a larger brown glass vial (100 mL volume). Dichloromethane (6 mL) was injected in the gap between the two vials and the larger vial was capped off with a plastic cap and parafilm. The vials were left undisturbed in an incubator at 20 °C. After 6 days, the crystals were harvested for single-crystal X-ray diffraction analysis. These crystals were washed three times with dry diethyl ether and were dried under reduced pressure at RT.

For the growth of the single-crystals with an empirical formula of (Bit-C3)<sub>4</sub>Pb<sub>3</sub>I<sub>10</sub> using the anti-solvent vapor crystallization approach,<sup>43</sup> stoichiometric amounts [targeted (Bit-C3)<sub>2</sub>PbI<sub>3.8</sub>Br<sub>0.2</sub> structure] of (Bit-C3)NH<sub>3</sub>I (0.038 mmol), PbI<sub>2</sub> (0.019 mmol), (Bit-C3)NH<sub>3</sub>Br (0.002 mmol), and PbBr<sub>2</sub> (0.001 mmol) were dissolved in dry GBL (0.379 mL) under continuous stirring at 60 °C for 30 min. The precursor solution was filtered through a syringe filter (0.2 μm mash) and transferred to a small glass vial (20 mL volume). The small vial was put in a larger brown glass vial (100 mL volume). Dichloromethane (10 mL) was injected in the gap between the two vials and the larger vial was capped off with a plastic cap and parafilm. The vials were left undisturbed in an incubator at 20 °C. After 7 days, the crystals were harvested for single-crystal X-ray diffraction analysis. These crystals were washed three times with dry diethyl ether and were dried under reduced pressure at RT.

**Thin film deposition.** All precursor solutions were filtered through a PTFE syringe filter (0.45 μm mash). Quartz substrates were cleaned through successive steps in the following order of solvents (detergent water, deionized water, acetone, and isopropanol; 15 min for each step), followed by a UV-ozone treatment of 15 min. The precursor solutions were deposited as thin films on quartz substrates by spin coating *via* a one-step method and annealed on a hotplate in a glove box under a nitrogen atmosphere (< 0.1 ppm O<sub>2</sub>, < 0.1 ppm H<sub>2</sub>O). Afterward, the samples were kept in a glovebox and only removed for analysis.

**(Bit-C3)<sub>2</sub>PbX<sub>4</sub> (with X=Cl, Br, and I):** Stoichiometric amounts of (Bit-C3)NH<sub>3</sub>X and PbX<sub>2</sub> (with X= Cl, Br, and I) were dissolved in dry DMF (0.3 M) under continuous stirring at 40 °C for 30 min. Due to the reduced solubility of (Bit-C3)NH<sub>3</sub>Cl in dry DMF, the precursor solution of (Bit-C3)<sub>2</sub>PbCl<sub>4</sub> was prepared in a mixture of dry DMF:DMSO 2:1 (0.3 M). The thin films were thermally annealed at 150 °C for 15 min. For the *in-situ* measurements, the thin films were thermally annealed at 30°C for 5 min. Spin-coating: 2000 rpm, 2000 rpm/s, 20 s

**(Bit-C3)NH<sub>3</sub>X (with X= Cl, Br, and I):** (Bit-C3)NH<sub>3</sub>X was dissolved in dry DMF (0.6 M). The thin films were dried at 30 °C for 5 min. Spin-coating: 2000 rpm, 2000 rpm/s, 20 s

**(Bit-C3)<sub>2</sub>PbI<sub>4-4x</sub>Br<sub>4x</sub> (with x= 0.05, 0.025, 0.05, 0.25, 0.5, and 0.75):** Stoichiometric amounts of (Bit-C3)NH<sub>3</sub>X and PbX<sub>2</sub> (with X= Br and I) were dissolved in dry DMF (0.15 M) under continuous stirring at 40 °C for 30 min. The thin films were thermally annealed at 150 °C for 15 min. Spin-coating: 1000 rpm, 1000 rpm/s, 20 s

**Characterization.** Optical absorption spectra were measured on a Cary 5000 UV-Vis-NIR spectrophotometer from Agilent Technologies; a cleaned quartz substrate was used as a calibration background. PL emission spectra were measured with a Horiba-Jobin Yvon Fluorolog-3 spectrofluorometer equipped with double-grating excitation and emission monochromators and a 450 W Xe lamp as light source. An excitation wavelength of either 300 or 430 nm was used (as indicated in the figure captions). For temperature-controlled UV-Vis, precursor solutions were spin-coated onto a cleaned quartz disk and transferred to a temperature-controlled cell (custom made by Harrick Scientific Products, New York). The temperature was controlled using a temperature-controller from Watlow®. The temperature of the film is measured with a thermocouple touching the film. A heating ramp of 1 °C/min was used for the measurements. After the heating ramp, the system is left to cool down naturally to room temperature (only data points during the

ramping period were used). The measurements were conducted under a nitrogen gas flow.

X-ray diffraction measurements were performed at room temperature in an ambient atmosphere on a Bruker D8 Discover diffractometer with a parallel beam geometry using a Göbel mirror and CuK<sub>α</sub> radiation, with an energy-dispersive one-dimensional detector (Lynxeye). Temperature-controlled XRD measurements were performed on the same instrument with a temperature cell under a nitrogen flow. Patterns were measured at temperatures separated by 10 °C, starting at 30 °C till 210 °C. A heating ramp of 1 °C/min was used, followed by an isothermal period of 10 min to measure each pattern.

## ASSOCIATED CONTENT

The Supporting Information is available free of charge on the ACS Publications website.

Experimental details of the organic synthesis, single-crystal XRD measurements, single-crystal crystallographic information, absorption and emission spectra, and *in-situ* temperature-controlled UV-Vis absorption, and XRD measurements (PDF)

## AUTHOR INFORMATION

### Author Contributions

The manuscript was written through contributions of all authors. Paul-Henry Denis and Martijn Mertens contributed equally to this work as shared first authors<sup>†</sup>. All authors have given approval to the final version of the manuscript.

### Notes

The authors declare no competing financial interest.

## ACKNOWLEDGMENT

The FWO is acknowledged for the funding of research. P.-H.D. is a special research fund (BOF) doctoral (Ph.D.) student at UHasselt/IMO, and M.M. is an SB Ph.D. fellow at FWO (Number 1S20118N). W.T.M.V.G., L.L., and D.V. acknowledge the FWO for the funding of the SBO project PROCEED (FWO-S002019N) and the senior FWO research project G043320N. KVH thanks the Research Foundation – Flanders (FWO) (projects AUGÉ/11/029 and G099319N) for funding. The work has been carried out in the context of the solliance network ([www.solliance.eu](http://www.solliance.eu)), from which UHasselt is a member. Additionally, UHasselt is a partner in the Energyville Consortium (<http://www.energyville.be/about-energyville>). Bart Ruttens and Jan D'Haen (IMO-IMOMEC) are acknowledged for XRD measurements. Maider Calderon Gonzalez is acknowledged for the research contribution during her bachelor thesis.

## REFERENCES

- (1) Grancini, G.; Nazeeruddin, M. K. Dimensional Tailoring of Hybrid Perovskites for Photovoltaics. *Nat. Rev. Mater.* **2019**, *4* (1), 4–22.
- (2) Lin, H.; Zhou, C.; Tian, Y.; Siegrist, T.; Ma, B. Low-Dimensional Organometal Halide Perovskites. *ACS Energy Lett.* **2018**, *3* (1), 54–62.
- (3) Mao, L.; Stoumpos, C. C.; Kanatzidis, M. G. Two-Dimensional Hybrid Halide Perovskites: Principles and Promises. *J. Am. Chem. Soc.* **2019**, *141* (3), 1171–1190.
- (4) Thrithamarassery Gangadharan, D.; Ma, D. Searching for Stability at Lower Dimensions: Current Trends and Future Prospects of Layered Perovskite Solar Cells. *Energy Environ. Sci.* **2019**, *12* (10), 2860–2889.
- (5) Stoumpos, C. C.; Cao, D. H.; Clark, D. J.; Young, J.; Rondinelli, J. M.; Jang, J. I.; Hupp, J. T.; Kanatzidis, M. G. Ruddlesden-Popper Hybrid Lead Iodide Perovskite 2D Homologous Semiconductors. *Chem. Mater.* **2016**, *28* (8), 2852–2867.
- (6) Soe, C. M. M.; Nie, W.; Stoumpos, C. C.; Tsai, H.; Blancon, J.-C.; Liu, F.; Even, J.; Marks, T. J.; Mohite, A. D.; Kanatzidis, M. G. Understanding Film Formation Morphology and Orientation in High Member 2D Ruddlesden-Popper Perovskites for High-Efficiency Solar Cells. *Adv. Energy Mater.* **2018**, *8* (1), 1700979.
- (7) Smith, I. C.; Hoke, E. T.; Solis-Ibarra, D.; McGehee, M. D.; Karunadasa, H. I. A Layered Hybrid Perovskite Solar-Cell Absorber with Enhanced Moisture Stability. *Angew. Chemie Int. Ed.* **2014**, *53* (42), 11232–11235.
- (8) Saparov, B.; Mitzi, D. B. Organic-Inorganic Perovskites: Structural Versatility for Functional Materials Design. *Chem. Rev.* **2016**, *116* (7), 4558–4596.
- (9) Que, C.-J.; Mo, C.-J.; Li, Z.-Q.; Zhang, G.-L.; Zhu, Q.-Y.; Dai, J. Perovskite-Like Organic-Inorganic Hybrid Lead Iodide with a Large Organic Cation Incorporated within the Layers. *Inorg. Chem.* **2017**, *56* (5), 2467–2472.
- (10) Liu, C.; Huhn, W.; Du, K.-Z.; Vazquez-Mayagoitia, A.; Dirkes, D.; You, W.; Kanai, Y.; Mitzi, D. B.; Blum, V. Tunable Semiconductors: Control over Carrier States and Excitations in Layered Hybrid Organic-Inorganic Perovskites. *Phys. Rev. Lett.* **2018**, *121* (14), 146401.
- (11) Braun, M.; Tuffentsammer, W.; Wachtel, H.; Wolf, H. C. Pyrene as Emitting Chromophore in Organic-Inorganic Lead Halide-Based Layered Perovskites with Different Halides. *Chem. Phys. Lett.* **1999**, *307* (5–6), 373–378.
- (12) Du, K.; Tu, Q.; Zhang, X.; Han, Q.; Liu, J.; Zauscher, S.; Mitzi, D. B. Two-Dimensional Lead(II) Halide-Based Hybrid Perovskites Templated by Acene Alkylamines: Crystal Structures, Optical Properties, and Piezoelectricity. *Inorg. Chem.* **2017**, *56* (15), 9291–9302.
- (13) Lermer, C.; Harm, S. P.; Birkhold, S. T.; Jaser, J. A.; Kutz, C. M.; Mayer, P.; Schmidt-Mende, L.; Lotsch, B. V. Benzimidazolium Lead Halide Perovskites: Effects of Anion Substitution and Dimensionality on the Bandgap. *Zeitschrift für Anorg. und Allg. Chemie* **2016**, *642* (23), 1369–1376.
- (14) Shi, E.; Yuan, B.; Shiring, S. B.; Gao, Y.; Akriti; Guo, Y.; Su, C.; Lai, M.; Yang, P.; Kong, J.; et al. Two-Dimensional Halide Perovskite Lateral Epitaxial Heterostructures. *Nature* **2020**, *580* (7805), 614–620.
- (15) Wang, Z.; Ganose, A. M.; Niu, C.; Scanlon, D. O. Two-Dimensional Eclipsed Arrangement Hybrid Perovskites for Tunable Energy Level Alignments and Photovoltaics. *J. Mater. Chem. C* **2019**, *7* (17), 5139–5147.
- (16) Mitzi, D. B.; Chondroudis, K.; Kagan, C. R. Design, Structure, and Optical Properties of Organic-Inorganic Perovskites Containing an Oligothiophene Chromophore. *Inorg. Chem.* **1999**, *38* (26), 6246–6256.
- (17) Herckens, R.; Van Gompel, W. T. M.; Song, W.; Gélvez-Rueda, M. C.; Maufort, A.; Ruttens, B.; D'Haen, J.; Grozema, F. C.; Aernouts, T.; Lutsen, L.; et al. Multi-Layered Hybrid Perovskites Templated with Carbazole Derivatives: Optical Properties, Enhanced Moisture Stability and Solar Cell Characteristics. *J. Mater. Chem. A* **2018**, *6* (45), 22899–22908.
- (18) Van Gompel, W. T. M.; Herckens, R.; Denis, P.-H.; Mertens, M.; Gélvez-Rueda, M. C.; Van Hecke, K.; Ruttens, B.; D'Haen, J.; Grozema, F. C.; Lutsen, L.; et al. 2D Layered Perovskite Containing Functionalised Benzothieno-Benzothiophene Molecules: Formation, Degradation, Optical Properties and Photoconductivity. *J. Mater. Chem. C* **2020**, *8* (21), 7181–7188.
- (19) Van Gompel, W. T. M.; Herckens, R.; Van Hecke, K.; Ruttens, B.; D'Haen, J.; Lutsen, L.; Vanderzande, D. Towards 2D Layered Hybrid Perovskites with Enhanced Functionality: Introducing Charge-Transfer Complexes via Self-Assembly. *Chem. Commun.* **2019**, *55* (17), 2481–2484.
- (20) Van Gompel, W. T. M.; Herckens, R.; Van Hecke, K.; Ruttens, B.; D'Haen, J.; Lutsen, L.; Vanderzande, D. Low-Dimensional Hybrid Perovskites Containing an Organic Cation with an Extended Conjugated System: Tuning the Excitonic Absorption Features. *ChemNanoMat* **2019**, *5* (3), 323–327.
- (21) Marchal, N.; Van Gompel, W.; Gélvez-Rueda, M. C.; Vandewal, K.; Van Hecke, K.; Boyen, H.-G.; Conings, B.; Herckens, R.; Maheshwari, S.; Lutsen, L.; et al. Lead-Halide Perovskites Meet Donor-Acceptor Charge-Transfer Complexes. *Chem. Mater.* **2019**, *31* (17), 6880–6888.
- (22) Gélvez-Rueda, M. C.; Van Gompel, W. T. M.; Herckens, R.; Lutsen, L.; Vanderzande, D.; Grozema, F. C. Inducing Charge Separation in Solid-State Two-Dimensional Hybrid Perovskites

- through the Incorporation of Organic Charge-Transfer Complexes. *J. Phys. Chem. Lett.* **2020**, *11* (3), 824–830.
- (23) Hu, H.; Meier, F.; Zhao, D.; Abe, Y.; Gao, Y.; Chen, B.; Salim, T.; Chia, E. E. M.; Qiao, X.; Deibel, C.; et al. Efficient Room-Temperature Phosphorescence from Organic-Inorganic Hybrid Perovskites by Molecular Engineering. *Adv. Mater.* **2018**, *30* (36), 1707621.
- (24) Hu, H.; Zhao, D.; Gao, Y.; Qiao, X.; Salim, T.; Chen, B.; Chia, E. E. M.; Grimsdale, A. C.; Lam, Y. M. Harvesting Triplet Excitons in Lead-Halide Perovskites for Room-Temperature Phosphorescence. *Chem. Mater.* **2019**, *31* (7), 2597–2602.
- (25) Roncali, J.; Leriche, P.; Blanchard, P. Molecular Materials for Organic Photovoltaics: Small Is Beautiful. *Adv. Mater.* **2014**, *26* (23), 3821–3838.
- (26) Mishra, A.; Ma, C.-Q.; Bäuerle, P. Functional Oligothiophenes: Molecular Design for Multidimensional Nanoarchitectures and Their Applications †. *Chem. Rev.* **2009**, *109* (3), 1141–1276.
- (27) Dunlap-Shohl, W. A.; Barraza, E. T.; Barrette, A.; Dovletgeldi, S.; Findik, G.; Dirkes, D. J.; Liu, C.; Jana, M. K.; Blum, V.; You, W.; et al. Tunable Internal Quantum Well Alignment in Rationally Designed Oligomer-Based Perovskite Films Deposited by Resonant Infrared Matrix-Assisted Pulsed Laser Evaporation. *Mater. Horizons* **2019**, *6* (8), 1707–1716.
- (28) Gao, Y.; Shi, E.; Deng, S.; Shiring, S. B.; Snaider, J. M.; Liang, C.; Yuan, B.; Song, R.; Janke, S. M.; Liebman-Peláez, A.; et al. Molecular Engineering of Organic–Inorganic Hybrid Perovskites Quantum Wells. *Nat. Chem.* **2019**, *11* (12), 1151–1157.
- (29) Jana, M. K.; Janke, S. M.; Dirkes, D. J.; Dovletgeldi, S.; Liu, C.; Qin, X.; Gundogdu, K.; You, W.; Blum, V.; Mitzi, D. B. Direct-Bandgap 2D Silver–Bismuth Iodide Double Perovskite: The Structure-Directing Influence of an Oligothiophene Spacer Cation. *J. Am. Chem. Soc.* **2019**, *141* (19), 7955–7964.
- (30) Deng, S.; Snaider, J. M.; Gao, Y.; Shi, E.; Jin, L.; Schaller, R. D.; Dou, L.; Huang, L. Long-Lived Charge Separation in Two-Dimensional Ligand-Perovskite Heterostructures. *J. Chem. Phys.* **2020**, *152* (4), 044711.
- (31) Zhu, X.-H.; Mercier, N.; Frère, P.; Blanchard, P.; Roncali, J.; Allain, M.; Pasquier, C.; Riou, A. Effect of Mono- versus Di-Ammonium Cation of 2,2'-Bithiophene Derivatives on the Structure of Organic–Inorganic Hybrid Materials Based on Iodo Metallates. *Inorg. Chem.* **2003**, *42* (17), 5330–5339.
- (32) Mitzi, D. B.; Chondroudis, K.; Kagan, C. R. Organic-Inorganic Electronics. *IBM J. Res. Dev.* **2001**, *45* (1), 29–45.
- (33) Kamminga, M. E.; Fang, H.-H.; Filip, M. R.; Giustino, F.; Baas, J.; Blake, G. R.; Loi, M. A.; Palstra, T. T. M. Confinement Effects in Low-Dimensional Lead Iodide Perovskite Hybrids. *Chem. Mater.* **2016**, *28* (13), 4554–4562.
- (34) Billing, D. G.; Lemmerer, A. Inorganic–Organic Hybrid Materials Incorporating Primary Cyclic Ammonium Cations: The Lead Iodide Series. *CrystEngComm* **2007**, *9* (3), 236–244.
- (35) Passarelli, J. V.; Fairfield, D. J.; Sather, N. A.; Hendricks, M. P.; Sai, H.; Stern, C. L.; Stupp, S. I. Enhanced Out-of-Plane Conductivity and Photovoltaic Performance in  $n = 1$  Layered Perovskites through Organic Cation Design. *J. Am. Chem. Soc.* **2018**, *140* (23), 7313–7323.
- (36) Smith, M. D.; Jaffe, A.; Dohner, E. R.; Lindenberg, A. M.; Karunadasa, H. I. Structural Origins of Broadband Emission from Layered Pb–Br Hybrid Perovskites. *Chem. Sci.* **2017**, *8* (6), 4497–4504.
- (37) Papadatos, D.; Vassilakopoulou, A.; Koutselas, I. Energy Transfer Yellow Light Emitting Diodes Based on Blends of Quasi-2D Perovskites. *J. Lumin.* **2017**, *188* (January), 567–576.
- (38) Grancini, G.; Srimath Kandada, A. R.; Frost, J. M.; Barker, A. J.; De Bastiani, M.; Gandini, M.; Marras, S.; Lanzani, G.; Walsh, A.; Petrozza, A. Role of Microstructure in the Electron–Hole Interaction of Hybrid Lead Halide Perovskites. *Nat. Photonics* **2015**, *9* (10), 695–701.
- (39) Yuan, M.; Quan, L. N.; Comin, R.; Walters, G.; Sabatini, R.; Voznyy, O.; Hoogland, S.; Zhao, Y.; Beauregard, E. M.; Kanjanaboos, P.; et al. Perovskite Energy Funnels for Efficient Light-Emitting Diodes. *Nat. Nanotechnol.* **2016**, *11* (10), 872–877.
- (40) Braun, M.; Tuffentsammer, W.; Wachtel, H.; Wolf, H. C. Tailoring of Energy Levels in Lead Chloride Based Layered Perovskites and Energy Transfer between the Organic and Inorganic Planes. *Chem. Phys. Lett.* **1999**, *303* (1–2), 157–164.
- (41) Andrzejak, M.; Witek, H. A. The Elusive Excited States of Bithiophene: A CASPT2 Detective Story. *Theor. Chem. Acc.* **2011**, *129* (2), 161–172.
- (42) Cao, D. H.; Stoumpos, C. C.; Farha, O. K.; Hupp, J. T.; Kanatzidis, M. G. 2D Homologous Perovskites as Light-Absorbing Materials for Solar Cell Applications. *J. Am. Chem. Soc.* **2015**, *137* (24), 7843–7850.
- (43) Shi, D.; Adinolfi, V.; Comin, R.; Yuan, M.; Alarousu, E.; Buin, A.; Chen, Y.; Hoogland, S.; Rothenberger, A.; Katsiev, K.; et al. Low Trap-State Density and Long Carrier Diffusion in Organolead Trihalide Perovskite Single Crystals. *Science* (80-. ). **2015**, *347* (6221), 519–522.
- (44) Mitzi, D. B. Templating and Structural Engineering in Organic–Inorganic Perovskites. *J. Chem. Soc. Dalton Trans.* **2001**, No. 1, 1–12.
- (45) Ma, D.; Xu, Z.; Wang, F.; Deng, X. Syntheses of Two-Dimensional Propylammonium Lead Halide Perovskite Microstructures by a Solution Route. *CrystEngComm* **2019**, *21* (9), 1458–1465.
- (46) Song, Z.; Wathage, S. C.; Phillips, A. B.; Tompkins, B. L.; Ellingson, R. J.; Heben, M. J. Impact of Processing Temperature and Composition on the Formation of Methylammonium Lead Iodide Perovskites. *Chem. Mater.* **2015**, *27* (13), 4612–4619.
- (47) Mitzi, D. B. A Layered Solution Crystal Growth Technique and the Crystal Structure of (C6H5C2H4NH3)2PbCl4. *J. Solid State Chem.* **1999**, *145* (2), 694–704.
- (48) Pradeesh, K.; Nageswara Rao, K.; Vijaya Prakash, G. Synthesis, Structural, Thermal and Optical Studies of Inorganic–Organic Hybrid Semiconductors, R-Pb1 4. *J. Appl. Phys.* **2013**, *113* (8), 083523.
- (49) Papavassiliou, G. C.; Koutselas, I. B. Structural, Optical and Related Properties of Some Natural Three- and Lower-Dimensional Semiconductor Systems. *Synth. Met.* **1995**, *71* (1–3), 1713–1714.

